



Determination of regions prone to sand production and the linkage to fluid flow rates by integrating rock strength parameters and microphotographs in the southern onshore basin, India

Ankita Kukshal¹ · Ravi Sharma¹ · Hirak Jyoti Kalita¹ · G. M. Yeshwanth¹ · Varun Dev Jamwal¹ · Hari Lal²

Received: 1 December 2022 / Accepted: 17 November 2023 / Published online: 22 December 2023
© The Author(s) 2023

Abstract

One of the main challenges for healthy hydrocarbon yields from the production wells is the sand production, and its control assumes significant importance for successful production operations. The prime objective remains to control the sand production without compromising on the fluid flow rates. Sand production is conventionally associated with diverse heterogeneous formations, especially poorly consolidated formations. Scrutinizing fluid flow rates at different orientations of perforations is a valuable analysis in controlling the sand production. This study was conducted to examine the case of sand production in a few development wells from Malleshwaram field of the Krishna Godavari (KG) basin in south India and provide alternatives to arrest this sand production. The influence of oriented perforations on fluid flow rates to minimize sanding tendencies was examined. Sand grain diameter was estimated using the distribution plots of the grain sizes obtained from the photomicrographs, and the average value of the grain size was estimated around 100 μm . The fluid flow model was simulated for actual scenario in the hydrocarbon bearing Nandigama formation using finite element modeling (FEM). Sanding tendencies in these formations were studied at varying depletion rates. Critical draw down pressure (CDDP), which is a function of both critical bottom hole pressure and reservoir pore pressure, for well 1 and well 2 is estimated as 4650 Psi and 3400 Psi, respectively, at 0% depletion. CDDP was used to estimate the onset of sanding, and the flow rate for horizontal perforation was calculated as 0.024548 m^3/sec . Strength parameters, namely the unconfined compressive strength (UCS) and cohesion, were also investigated in all the wells to decipher the formation strength and a possible linkage to sanding. These results present a completely fresh analysis of the sanding potential and the related parameters responsible for it in these formations. Fluid flow rates for the producing reservoir are studied at different set of oriented and sized perforations. It was observed that a hiked flow rate in horizontal perforations maintains the production in a safe and no-sanding zone. This study provides vital information and a workflow for similar heterogeneous complex formations for designing the well completions, augmenting economic production and reinforcing future reservoir management.

Keywords Fluid flow · Finite element modeling · Hydrocarbon and sand production · Oriented perforation

List of symbols

E_{dyn} Dynamic Young's modulus in Psi
 E_s Static Young's modulus in Psi

This paper is intended for publication in the Journal of Petroleum Exploration and Petroleum Technology.

✉ Ravi Sharma
ravi.sharma@es.iitr.ac.in

¹ Department of Earth Sciences, Indian Institute of Technology Roorkee, Roorkee, Uttarakhand 247667, India

² Oil and Natural Gas Corporation Limited, Dehradun, Uttarakhand 248003, India

g Acceleration due to gravity in cm/sec^2
 G_{dyn} Dynamic shear modulus in Psi
 K_{dyn} Dynamic bulk modulus in Psi
 P_H Hydrostatic pore pressure in Psi
 P_p Pore pressure in Psi
 S_v Vertical stress in Psi
 α Biot's coefficient, unitless
 Δt_p Compressional transit time in $\mu\text{sec}/\text{foot}$
 Δt_s Shear transit time in $\mu\text{sec}/\text{foot}$
 Δt_{normal} Slowness of normal compaction trend line in $\mu\text{sec}/\text{foot}$
 ε_h Minimum horizontal strain, unitless
 ε_H Maximum horizontal strain, unitless
 ρ_b Bulk density in g/cc

σ_h	Minimum horizontal stress in Psi
σ_H	Maximum horizontal stress in Psi
ν	Poisson's ratio, unitless

Introduction

In the oil and gas sector, millions of dollars are spent on cleaning sand to hamper its rising repercussions all around the globe (Willson 2002). Sand production poses a global problem regarding economic losses and high nonproduction time (Tremblay 1996). It severely affects the entire life cycle of the reservoir and well. Sand production, especially from unconsolidated formation reservoirs, is a major challenging issue that restricts the production flow rate (Salahi et al. 2021) and the economy. Incessant sand production accumulates in surface tools, wellbores, pipelines, separators, and tubing, resulting in decreased production and economic losses (Morita and Boyd 1991). It causes erosion of the downhole facilities and exposure to hydrocarbon further enhances the corrosion (Mahmud et al. 2020). It also possesses geomechanical problems, including formation damage, excess of which causes a void behind the casing leading to collapsing overlying layers (Rahman et al. 2010; Abdelghany et al. 2023). This damage to subsurface equipment and surface facilities leads to safety and environmental concerns (Sanfilippo et al. 1995; Tabar et al. 2021). Sand production commences when the stress on the formation overshoots the formation's strength and leads to rock failures (Dehghani 2016; Vincent et al. 2012; Weigarten and Perkins 1995; Aroyehun et al. 2018; Ismail et al. 2020). Figure 1 shows the sand production mechanism involving three steps: near wellbore damage, perforation, and transportation.

Factors affecting formation propensity to produce sand can be classified into two categories, fluid flow and rock strength effects. Broadly, sand particle production

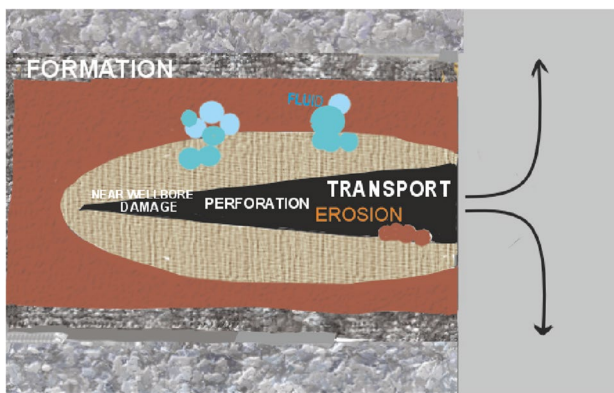


Fig. 1 Schematics representing the three-step process for sand production includes near wellbore damage, perforation, and transportation

can comprise load-bearing solids and formation fines (Matanovic et al. 2012; Issa et al. 2022). The production of formation fines not in the range of mechanical formation is crucial as they can be transported easily within the formation instead of plugging it (Mahmud and Abdullah 2017; Vaziri et al. 2002). The production rate is consistently maintained low to cease the production of particles, whereas in many situations low production rate is considered uneconomical and inefficient (Mahmud et al. 2020; McLellan et al. 2000). These factors can be classified as below.

The degree of consolidation throws light on how strongly single sand grains are bound together (Vaziri et al. 1998). Generally, the secondary geological process affects and causes sandstone cementation. Also, the overlying sediments impact force in the deeper region, making it tighter and more consolidated than the younger unconsolidated sediments lying in shallow formations (Tronvoll 1997). Sand production is a significant problem when producing from shallow unconsolidated formations. The young sedimentary formation has a relatively higher percentage of the material matrix that binds sand grains together; such formation is unconsolidated or poorly consolidated (Deng et al. 2013). Rock strength property is vital in defining the formation's degree of consolidation and strength (Ismail et al. 2020). Unconsolidated sandstone formation having formation strength less than 6.9 MPa is termed unconsolidated and leads to sand failures due to weak rock strength (Mahmud 2020).

Cutting the challenge of sand production to boost the production rate of reservoir fluid and improve the operational efficiency has become mandatory (Jin et al. 2012). The production of a reservoir hydrocarbon fluid gives rise to pressure friction losses and frictional forces due to the interplay of potential and kinetic energy that may go beyond the formation's compressive strength (Tovar 2018). Hence, the majority of production wells are bounded by critical flow rate. The critical flow rate is usually below frictional pressure losses and frictional forces and should not exceed the compressive strength of the formation (Bowes and Procter 1997). The critical flow rate is obtained by increasing the production rate slowly until the production of sand is detected (Vardoulakis et al. 1996). One technique to reduce sand production is using a choke valve that reduces the production rate to a critical rate where sand production follows acceptable limits or does not occur (Sulaimon and Teng 2020). Sometimes this flow is considerably less than the acceptable fluid flow for the production well (Mahmud and Abdullah 2017), and this hampers the economics. Sanding can be avoided by monitoring draw down and production rates slowly and in increasing steps to ensure that the draw-down is below the point at which formation grain may get loosed and detached (Jin et al. 2012).

The flow makes the frictional force act on the sand particles of reservoir fluid (Haimson and Chang 2000). The

frictional force is directly related to reservoir fluid viscosity and flow rate. Reservoir fluid with a higher viscosity usually applies a more significant frictional drag force to the formation particles than a low-viscosity fluid (Matanovic et al. 2012; Hussein and Ni 2018). Further, the viscous drag produces sand from heavy oil reservoirs containing a higher specific gravity and viscosity liquids despite low flow rates. Sand production increases with increasing water cuts (Papamichos et al. 2001; Moore 1994). During the sandstone formation being water-wet, some inter-particle cohesiveness is provided via the surface tension of connate water surrounding each sand particle. The onset of water production leads to innate adherence of the connate water with the produced water, thereby causing a decrease in the surface tension force (McLellan 2000). This ultimately leads to a reduction in particle-to-particle cohesiveness, poorly affecting the strength of the sand arch surrounding the perforation (Willson et al. 2002; Abduljabbar et al. 2022). Relative permeability also influences sand production. With increasing water cut, the relative permeability of oil decreases, causing an increase in differential pressure required to produce hydrocarbon fluid at the same rate (Pearson and Zazovsky 1997; Li et al. 2022). Increasing the differential pressure near the well bottom hole leads to higher shear force by forming sand particles resulting in sand arch instability around the perforation. Perforation orientation and size impact stress distribution around the wellbore depending on rock strength properties and behavior and play a crucial role in influencing stability and sand production. Perforation pattern and density reduce sand production with the highest fluid flow efficiency. Selective perforation favoring horizontal direction may avoid the sanding zones with increased fluid flow. Perforation patterns are more stable for spiral orientation than inline and in-plane (Subbiah 1997). It can be used to increase fluid flow rates without compromising the economics.

Several oil companies tend to take conventional techniques using preventative measures such as gravel-pack filters, slotted liners or downhole screens. Sometimes this equipment is unnecessarily installed as a preventative measure, causing increased production costs and decreased well's productivity. It increases complexity and is labor-intensive in nature. The process involves meticulous wellbore preparation, including the installation of screens or gravel packs, which can be time-consuming and costly. Many approaches have been developed to understand the sanding tendencies by employing physical model testing, analytical modeling, and numerical models (Rahmati et al. 2013; Deng et al. 2018). Laboratory tests that can only be conducted on recovered cores are relatively expensive and available for discrete depths only. Moreover, these tests are limited to predicting the onset of sand production only. Physical modeling can only predict volumetric sand production, yet

expensive and time-consuming (Papamichos et al. 2001). Analytical models are rapid and easily operated, but they are limited to speculating the onset of sand production and may not reflect real-world conditions accurately. They may not be suitable for reservoirs with complex geometries, multiple layers, or unconventional formations. Chemical sand control methods are versatile and encompass a broader range of approaches, from the injection of consolidating resins to the application of scale inhibitors and wettability alteration agents (Madadzadeh et al. 2022a, 2022b). However, they possess potential environmental impact, which involves the injection of chemicals, such as acids, scale inhibitors, and solvents, into the reservoir, resulting in the dissolution of minerals within the reservoir rock, subsequently reducing permeability and hindering hydrocarbon recovery (Madadzadeh et al. 2022c; Tabar et al. 2021). Additionally, applying chemicals, particularly acids, can inadvertently damage the reservoir (Madadzadeh et al. 2022b). Hybrid methods aim to combine the benefits of both mechanical and chemical approaches but may inherit some of their respective disadvantages. For instance, a mechanical-chemical approach can involve the use of screens in conjunction with chemical consolidants. While it offers an innovative solution, it can still be affected by screen plugging and chemical compatibility issues. Several of the mentioned models are only valid for a single mechanism having simplified geometrical and boundary conditions, which are not usually the case in actual field conditions (Zolotukhin and Gayubov 2022). Numerical models are by far the most powerful tools for predicting sand production. They can provide insights and qualitative measurements that are difficult to obtain otherwise (Rahmati et al. 2013). Finite element method (FEM), easy and widely used, can model complex geometries, irregular shapes, and easily incorporates boundary conditions (Wang 2006).

This study was conducted in a few development wells from Malleshwaram, and the possibility of sanding and the influence of perforation on fluid flow rates to minimize sanding tendencies was examined. Also, fluid flow rates at critical draw down pressure were computed and analyzed for a different set of orientated perforations. The average diameter of the sand grain was computed using the histogram plot obtained from the photomicrographs and was found to be 100 μm . Strength parameters, namely the unconfined compressive strength (UCS) and cohesion, were investigated in all wells to decipher the formation strength. CDDP was computed at the increasing percentage of depletion to estimate the onset of sanding, and fluid flow rates were calculated for the same. Critical draw down pressure (CDDP), which is a function of both critical bottom hole pressure and reservoir pore pressure, for well 1 and well 2 is estimated as 4650 Psi and 3400 Psi, respectively, at 0% depletion. Petrophysical properties, namely porosity and permeability, were evaluated using He porosimeter while the pore pressure was calculated

using Eaton's formula. Reservoir having similar petrophysical properties were constructed using a total of 1,63,316 elements for mesh construction and mesh volume of 8.46 m^3 , and boundary conditions were defined to build the geometry. Fluid flow from the reservoir to the wellbore was simulated using Darcy law for laminar flow. The Navier–Stokes equation was generally used for free channel laminar flow. Finite element modeling using the actual reservoir condition was simulated and average fluid flow rate was calculated as $0.024548 \text{ m}^3/\text{sec}$. Fluid flow rates at different orientations and size were also simulated to scrutinize its influence. It was observed that horizontal perforation enhances the fluid flow rates appreciably without sanding tendencies.

Geological settings

Pericratonic Krishna Godavari Basin is a continental passive margin basin that came into existence following rifting along the eastern continental margin of the Indian craton in the early Mesozoic. The onland part consists of 2800 sq. km and is mostly alluvium covered (Bastia et al. 2006). The basin represents a fully developed passive margin sequence in the northern part and is characterized by a series of en echelon horst and graben systems, cascading down toward a thick pile of sediments of Permian to Recent age sagging in the southern part as shown in Fig. 2.

The sedimentary evolution of the KG basin can be divided into rift and drift phase. The syn-rift sequence is identified and described as Gollapalli, Kanukollu, and Nandigama and is seen throughout the basin (Rao and Mani 1993). Though no discernible unconformity is noticed between Gollapalli sandstone and Raghavapuram shale in the outcrop area, there is ample evidence from the subsurface geological and geophysical data that the rift-drift transition can be marked at the base of Raghavapuram shale. Since the Cretaceous times, the basin has become a pericratonic basin. Its thick fluvial load was associated with faulting of the basement

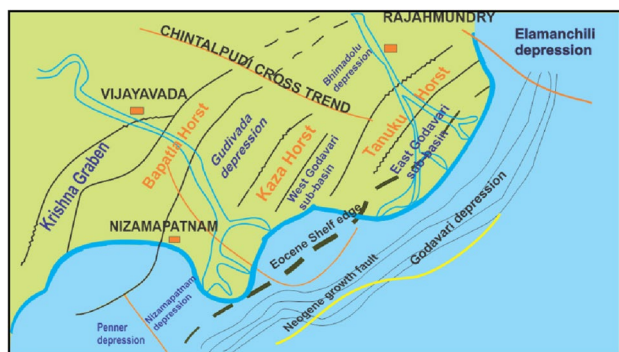


Fig. 2 Structural map showing major horst and graben structures in KG Basin (From, DGH Repository 2022)

block due to the re-activation of the NE-SW trending Precambrian faults (Bastia et al. 2006). These differential movements allowed magma to rise resulting in Razole volcanism. The present area falls within MS ML Block of KG onland and is situated in between the Kaza-Kaikalur horst in the west and Tanuku horst in the east of west Godavari sub-basin in Malleshwaram area. The location of the studied wells is marked on the map in Fig. 3

Well-1 is situated around 9 km north-west of well-2 and about 3 km north-east of well-3, in the Bantumilli graben falling under KG onland. These wells were drilled with a target depth of 3600 m. Well-3 was drilled vertically to a depth of 3700 m with a mud weight of 1.81 SG. The well penetrates about 2308 m of Tirupati sandstone and younger sediments, 1171 m of Raghavapuram shale and 615.5 m + of Nandigama formation. The studied well contains sediment ranging from Upper Jurassic to Cretaceous with shale acting as both source and trap while shale within form reservoir rocks as shown in Table 1.

Material and methods

Data availability

Conventional basic well log data, including gamma ray, density, neutron porosity, and calipers, were acquired for the studied wells. Production data, geological reports, drilling data, and well completion reports were also collected for the study area. Also, core plugs for the corresponding wells were utilized for photomicrographs and porosity estimations. Finally, an audit of all the data was conducted to review the quality, consistency, and suitability.

Methodology

The following steps were undertaken to form an integrated finite element model for fluid flow estimation:

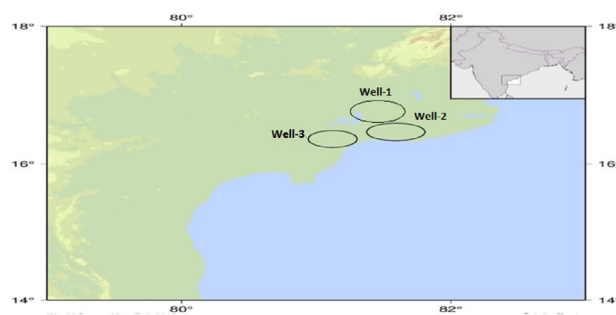


Fig. 3 Location map of the studied wells in KG Basin. The map is prepared by using CASMI, a visualization tool for the World Stress Map (WSM) database accessed by the online interface CASMO (Heidbach et al. 2018)

Table 1 Lithostratigraphic column of the KG Basin as encountered from the studied wells

Age	Formation	Lithology
Eocene-recent	Narsapur Claystone and Younger Nimmakuru Sandstone	Alteration of clay and sandstone. Dominantly sandstone with minute shale
Paleocene	Razole	Basalt with limestone, sandstone and clay
Upper cretaceous	Tirupati Sandstone	Dominant sandstone and claystone
Lower cretaceous	Raghavapuram Shale	Dominant clay with small amount of sandstone
L Jurassic-cretaceous	Nandigama formation	Sandstone with clay

1. Formation evaluation using sonic, neutron porosity and density log to qualitatively infer the formation lithology and porosity of the core plugs.
2. Creating mechanical earth model (MEM) using basic well log data set (GR log, sonic log and density log) to estimate pore pressure, elastic and strength properties.
3. Estimating grain size using the histogram distribution of photomicrographs obtained from scanning electron microscopy (SEM).
4. Using MEM, grain size and perforation details calculating critical draw down pressure at different percentage of depletion.
5. Sensitivity analysis of sanding in the sand prone depths and calculating the suitable range of critical drawdown pressure.
6. Finite element modeling using the actual field scenario and calculating the fluid flow rates at the reservoir conditions. Also calculating the flow rates at different depletion percentage to infer the critical flow rate.
7. Simulating the fluid flow using differently oriented perforation having phase angle of 36 degree in spiral configuration with different sizes to explore its influence.

Sand production analysis was conducted using basic well log data to predict the critical draw down pressure (CDDP), the minimum bottom hole pressure for which no solid particles are produced from a sand reservoir. A drawdown that is the difference between the reservoir pore pressure and the bottom hole pressure was formed, and a similar field production scenario was simulated using finite element modeling. During production, the reservoir pore pressure is depleted, and a drawdown is maintained and checked for the sanding tendencies for the studied formations. CDDP is influenced by the subsurface stress acting around the borehole and the strength possessed by the subsurface formations. Sanding analysis, therefore, requires an entire set of mechanical earth models, which is an encapsulation of subsurface stress and strength parameters, particularly unconfined compressive strength (UCS), along with the wellbore information like perforation details. Neutron porosity and density were also used to qualitatively infer the formation hardness and the cross-plot of two can help to distinguish between some

lithological type consisting of shale and sandstone (Yan et al. 2018). Lower density could suggest highly porous material for some formations as shown in Fig. 9a. The sonic log records the transit time and briefly elucidates the sand quality in the reservoir formation. Generally, if the travel time is shorter, sand is considered hard, having low porosity and high density. On the contrary, a longer travel time indicates that the sand is soft and has high porosity and low density.

Core plugs for the corresponding wells were analyzed to infer the porosity and grain density distribution. Helium was used with constant pressure and then expanded into the sample cell. The initial and final pressure was recorded to determine the sample pore volume and calculate the porosity. Formation porosity broadly refers to the degree of cementation in formation. It is a guiding factor to infer the amount of pore space, indirectly indicating inter-particle strength (Zhu et al. 2020). If the pore spaces are relatively higher and strength is relatively lesser, sand control in the formation could be needed (Ahad et al. 2020). Most samples have a relative density of 2.65, while the average sand size differs in production wells within the same formation. The grain size was therefore estimated using an experimental photomicrograph obtained from SEM analysis. A histogram was plotted to understand the grain size distribution in the SEM image and in a way in the studied subsurface formation. No literature was found using this approach to employ, the dominant grain size, 100 μm in this case, was used as an input to iteratively optimize the size and length of the perforation.

Routine logging operations involved in acquisition of logs such as density, sonic, and neutron logs to calculate reservoir formation potential have limited or no capacity to infer or predict the sand cut/production in the formations at certain levels of pressure drawdown. Integrated studies on core plugs and well log data were used as an effective tool for the evaluation of sanding tendency at different depletion percentages and computing the flow rates for the actual field conditions. In the production modeling, production is simulated by applying drawdown pressure at the wellbore and estimating the possible fluid flow at the critical drawdown pressure, which would avoid undesirable sanding. Increased perforation density and

orientation help to hinder sanding risk. More perforations increase the flow path for the hydrocarbon and the likelihood that the perforation will intersect the productive regions of an anisotropic reservoir (Crawford 1989). Next in line is the phasing because it gives a direct path to hydrocarbon to the wellbore when adequately chosen (Cosad 1992; Bell 1984). Proper perforation orientation escalates the fluid flow rates without compromising on the sanding tendencies. Sanding can be well managed by using differently oriented and sized perforations ranging from 0 to 360 degrees. Flow rates were computed to study the favorable direction, which gives the maximum fluid flow. The entire procedure is portrayed in the flow diagram, as shown in Fig. 4.

Rock elastic properties

Elastic parameters are computed using the conventional dipole sonic measurements (which includes compression slowness and shear slowness). Dynamic elastic properties namely shear modulus and bulk modulus can be determined directly by making use of the following mentioned Eqs. (1–5):

$$G_{\text{dyn}} = \frac{\rho_b}{(\Delta t_s)^2} \tag{1}$$

$$K_{\text{dyn}} = \rho_b \left[\frac{1}{(\Delta t_p)^2} \right] - \frac{4}{3} G_{\text{dyn}} \tag{2}$$

$$v = \frac{\rho_b \left(\frac{3}{\Delta t_p^2} \right) - \left(\frac{4}{\Delta t_s^2} \right)}{\left(\Delta t_s^2 \left(\frac{1}{\Delta t_p^2} \right) - \left(\frac{1}{\Delta t_s^2} \right) \right)} \tag{3}$$

$$E_{\text{dyn}} = \rho_b * \frac{\left(\frac{3}{\Delta t_p^2} \right) - \left(\frac{4}{\Delta t_s^2} \right)}{\Delta t_s^2 \left(\left(\frac{1}{\Delta t_p^2} \right) - \left(\frac{1}{\Delta t_s^2} \right) \right) * 10^{-12}} \tag{4}$$

where ρ_b is bulk density in g/cc. Δt_p is compressional slowness in $\mu\text{sec}/\text{foot}$ while Δt_s is shear slowness in $\mu\text{sec}/\text{foot}$, v is Poisson’s ratio, E_{dyn} is dynamic Young’s modulus in Psi, G_{dyn} is dynamic shear modulus in Psi and K_{dyn} is dynamic bulk modulus in Psi.

However, all these elastic properties are obtained from well log data and need to be changed to static parameters using the empirical equations for different lithologies encountered as given by Lacy (1997).

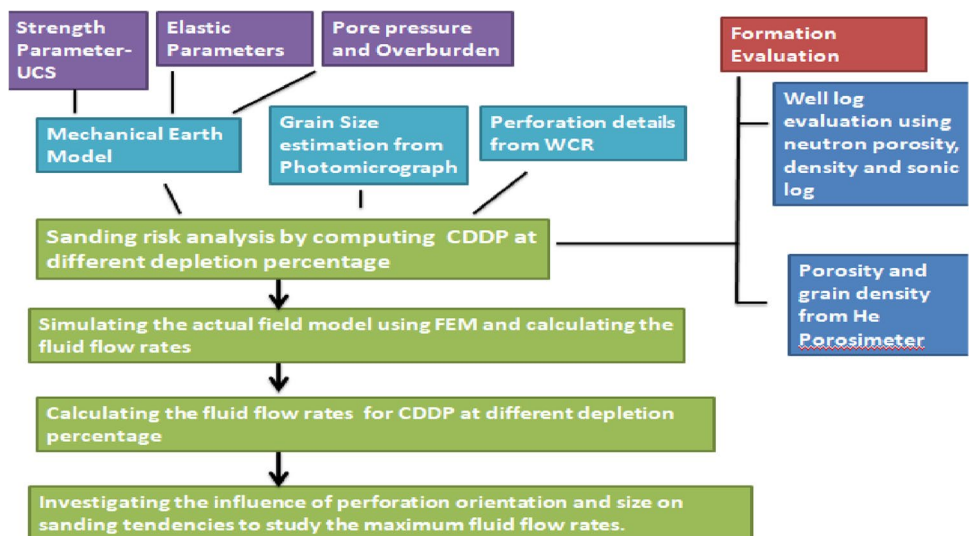
$$E_s = 0.018 E_{\text{dyn}}^2 + 0.422 E_{\text{dyn}} \tag{5}$$

Rock strength parameters

Rock strength constitutes a vital parameter in sand analysis and is dependent upon consolidation and unconsolidation of sediments. Unconsolidated sediments do increase chances for sand production (Plumb et al. 1992). Strength parameters are expressed in terms of unconfined compressive strength (UCS), and cohesion. UCS has a major say in defining the regions prone to sanding. Following Deere and Miller, Plumb (1994) developed a world-wide database for rocks typically encountered in sandstone reservoirs using static Young’s modulus as given by Eq. 6:

$$\text{UCS} = 2.280 + 4.1089E_s \tag{6}$$

Fig. 4 Flowchart showing the steps followed for analysis of sand production



where UCS is given in Psi, and E_s is static Young’s modulus in Psi.

Mechanical earth model

Mechanical earth model is an encapsulation of lithology, horizontal and vertical stress profile, pore pressure, elastic parameters and strength parameters. Overburden or vertical stress is the integration of the cumulative weight of overburden rocks as mentioned in Eq. 6. Plumb et al. (1994) provided the following equation to estimate the vertical stress using bulk density logs as:

$$S_V = \int_0^H \rho_b * g dH \tag{7}$$

where S_v is the vertical stress in Psi, ρ_b is the bulk density in g/cc, g is acceleration due to gravity in cm/s^2

Pore pressure as given by Eaton’s equation which uses a semi-logarithmic normal trend line (Zhang et al. 2011; Zhang et al. 2020). The various log measurements used by the Eaton Method are sonic or seismic interval velocity as given by Eq. 8:

$$P_p = S_V - (S_V - P_H) \left(\frac{\Delta t_{normal}}{\Delta t_p} \right)^3 \tag{8}$$

where P_p is reservoir pore pressure in Psi, P_H is hydrostatic pressure in Psi, S_V is total vertical stress in Psi and Δt_{normal} is slowness of normal compaction trend line in $\mu sec/foot$ while Δt_p is compressional slowness for onshore data in $\mu sec/foot$.

Also, horizontal strain components namely ϵ_h and ϵ_H which throws light on horizontal tectonic deformation. These are calculated as a function of overburden stress, Young’s modulus and Poisson’s ratio as given below in Eqs. (9–10) (Kidambi and Kumar 2016).

$$\epsilon_h = S_V \frac{\nu}{E_s} \left(\frac{1}{1-\nu} - 1 \right) \tag{9}$$

$$\epsilon_H = S_V \frac{\nu}{E_s \left(1 - \frac{\nu^2}{1-\nu} \right)} \tag{10}$$

where ϵ_h is the minimum horizontal strain and ϵ_H is the maximum horizontal strain, S_v is the overburden stress in Psi, E_s is static Young’s modulus in Psi, ν is Poisson’s ratio and is unitless.

Eventually, poro-elastic horizontal strain model was used to infer the horizontal stress magnitudes as given by Eqs. 11 and 12.

Table 2 Represents the input parameter for reservoir and wellbore used to create the working model

S.no	Parameter	Values
1	Reservoir radius	3 m
2	Reservoir thickness	0.3 m
3	Well radius	0.125 m
4	Perforation radius	0.025 m
5	Perforation length	0.08 m
8	Phase angle	1.2566
9	Pressure at perforations	1300 Psi
10	Reservoir pore pressure	8700 Psi
11	Permeability	1.613 mD
12	Viscosity	2.900 X 10 ⁻⁷ Psi. S
13	Fluid density	0.9 g/c
14	Porosity	0.1454

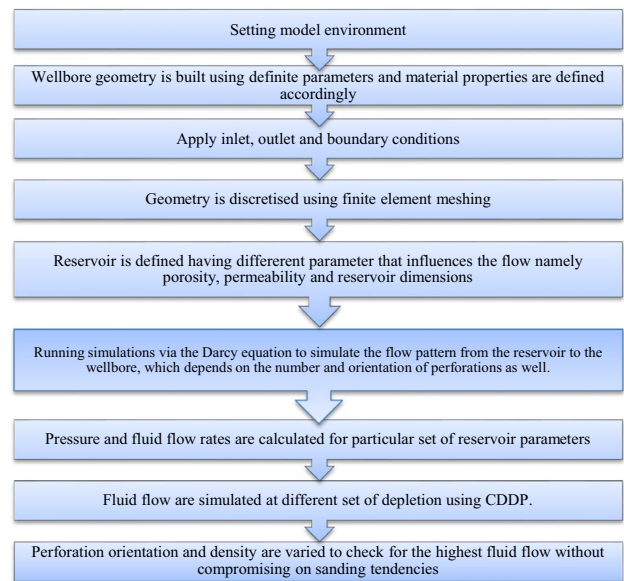


Fig. 5 Flowchart representing the procedure for simulating the fluid flow model

$$\sigma_h - \alpha P_p = \left(\frac{\nu}{1-\nu} \right) (S_v - \alpha P_p) + \frac{E_s \epsilon_h}{1-\nu^2} + \frac{E_s \epsilon_H}{1-\nu^2} \tag{11}$$

$$\sigma_H - \alpha P_p = \left(\frac{\nu}{1-\nu} \right) (S_v - \alpha P_p) + \frac{E_s \epsilon_H}{1-\nu^2} + \frac{E_s \epsilon_h}{1-\nu^2} \tag{12}$$

where E_s is Young’s modulus in Psi, ν is Poisson’s ratio and is unitless, σ_h is the minimum horizontal stress in Psi which is usually calibrated using the Leak off test (LOT) data available for the studied well, σ_H is the maximum horizontal stress in Psi, S_v is the vertical (overburden) stress in Psi, α is Biot’s constant assumed as one, ϵ_h is the minimum

Fig. 6 Photomicrograph (a, c, e) of the studied samples along with the histogram plots (b, d, f) displaying average grain size. The average grain size distribution is approximated as 100 μm which is taken as an input for sand analysis

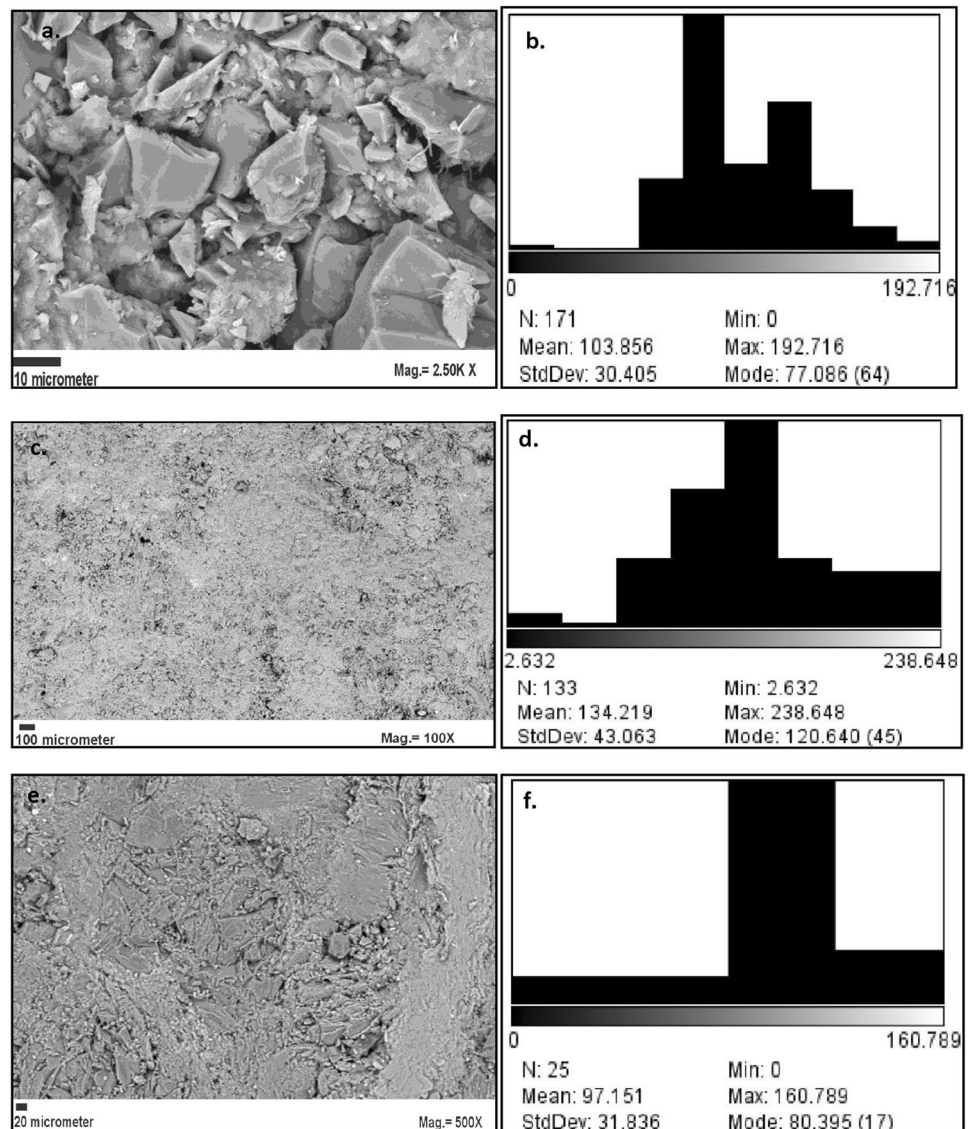


Table 3 Porosity and grain density estimated via porosimetry in studied core plugs

S.no	Chip ID/plug no	Porosity	Grain density (g/cc)
1	X-1	0.1639	2.66
2	X-2	0.1454	2.68
3	X-3	0.1587	2.68
4	X-4	0.1696	2.68
5	X-5	0.1599	2.66
6	X-6	0.1525	2.66
7	X-8	0.1397	2.74
8	2	0.1469	2.63

horizontal strain and ε_H is the maximum horizontal strain, P_p is pore pressure in Psi.

Sanding tendency prediction

Sanding onset conditions is specified with the help of critical drawdown, critical wellbore pressure and critical flow rate which are the production conditions at which failure criteria are fulfilled. Sanding tendencies for studied wells are inferred and critical draw down pressure (CDDP) are quantified for studied reservoir. It details the drawdown at which sanding commences at different depletion percentage.

CDDP is closely associated and function of in situ stress and pore pressure and so it is liable to change as the hydrocarbon are exploited. A profile was created for different depletion scenarios that range from 0 to 35 percentages that further throws light on the sanding tendencies for different formations encountered. Further, cross-plots between bottom hole flowing pressure and pore pressure were created as a function of depletion rate which gives a brief insight on

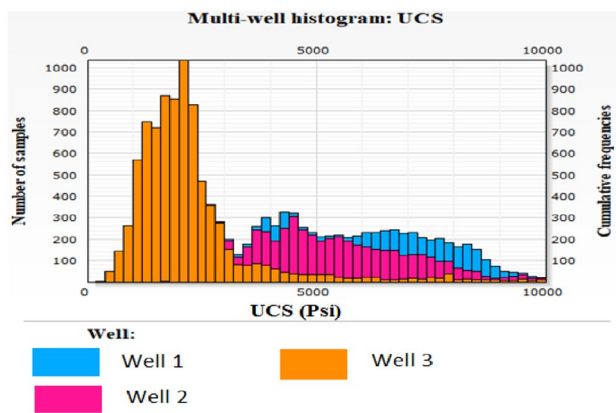


Fig. 7 The histogram portraying UCS of studied wells shown by different colors. The frequency of samples in well 3 is relatively higher with less magnitude relative to other wells with a higher magnitudes and lesser frequency

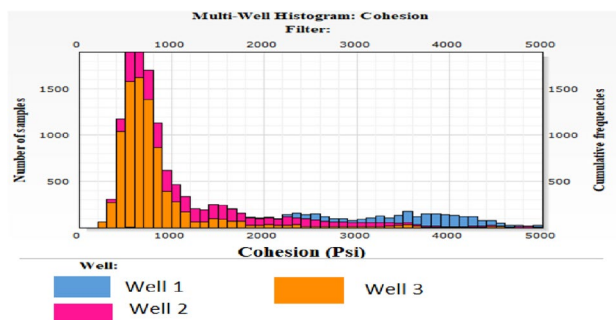


Fig. 8 The histogram portraying cohesion of studied wells shown by different colors. The frequency of samples in well 3 is relatively higher with less magnitude relative to other wells with a higher magnitudes and lesser frequency of samples as in well 1

sanding tendencies for a particular completion type over an entire reservoir section. This profile was of greater usage to completion engineer as it provided a range of suitable bottom hole pressure for particular reservoir pore pressure at a given depth to avoid sanding.

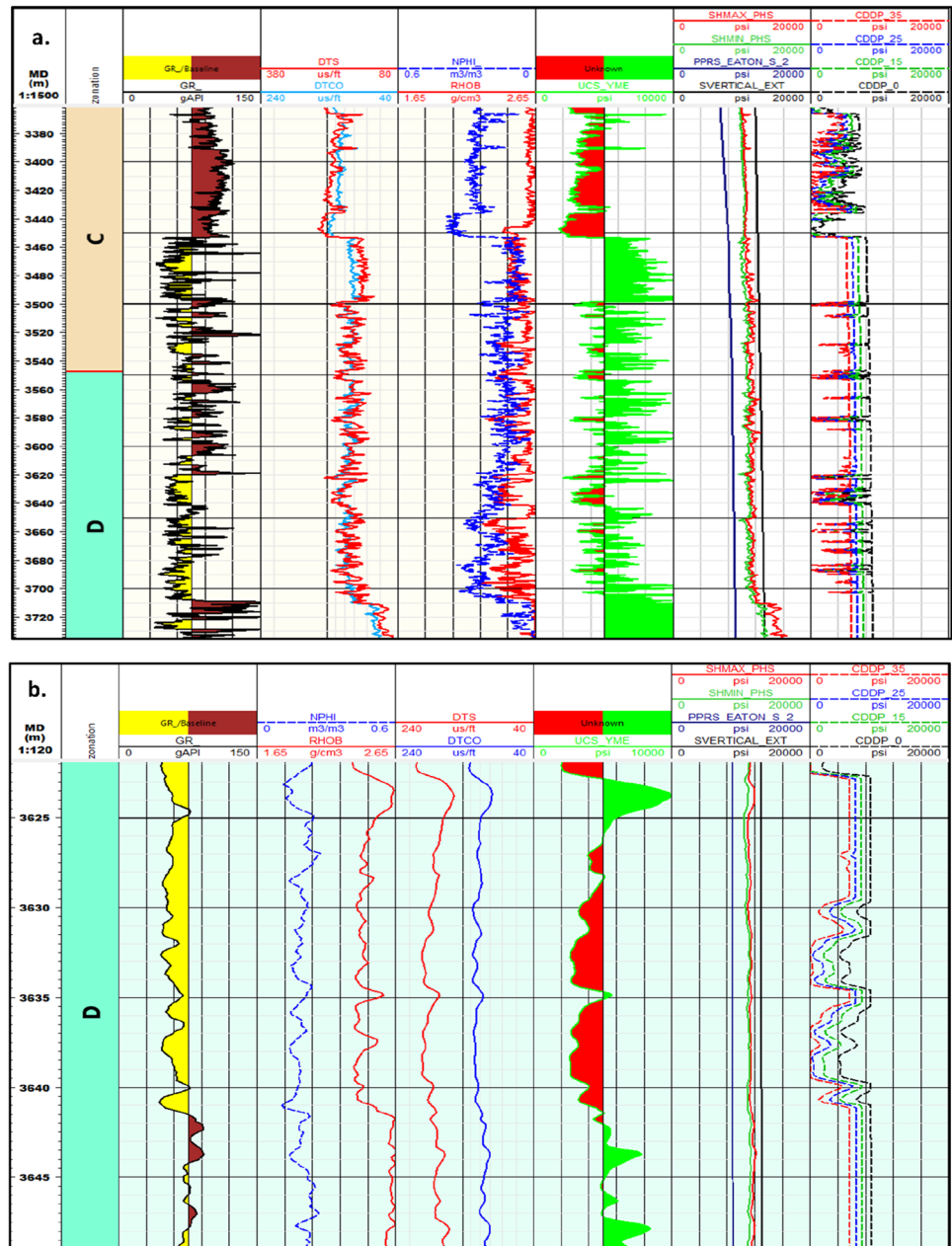
Fluid flow simulation using variable perforations

The finite element method was used to model fluid flows in porous media using Darcy's Law interface for laminar flow. For production modeling, Darcy's law was preferable since the significant driving force for the flow was the pressure gradient, and the momentum transfer by shear stresses within the fluid was negligible. Fluid flow from the reservoir to the wellbore was simulated using Darcy law for laminar flow. The Navier–Stokes equation was generally used for free channel

laminar flow. It governs the motion of fluids and represents the conservation of momentum. For the Navier–Stokes equation, streamlined diffusion was used for strongly coupled systems of equations. Streamline diffusion was crucial when convection dominates the flow, which was the case for this formation. The studied formation had low permeability in which finite elements were constructed for the entire wellbore and its periphery. Free surface triangular, tetrahedral elements, edge, and vertex elements were utilized for mesh construction and assumed that the dependent variable follows the polynomial function in the elements. A total of 1,63,316 elements were used for the mesh construction, with a mesh volume of 8.46 m³. More elements are used to create a finer mesh which takes much computing power to solve, thereby increasing the accuracy of results. During sand production, a sand zone is formed around the periphery of the perforations. Meshing can be beneficial in such processes where the geometry or the boundary is changing. Finite element methods have been mainly used to model heterogeneous cases with different parameter distributions. Boundary conditions are defined to the built geometry. The fluid was allowed to enter from the left entrance of the perforation with the velocity depending on the Reynolds number, and it gets open to the wellbore, where the pressure was taken to be zero with the condition that no back fluid flow would be allowed. The upper and the lower boundaries of the perforation built by two parallel plates were the walls with slip conditions applied to observe zero viscosity near the boundary. The flow efficiency of a wellbore completion is a factor of two parameters including the pressure differential and the perforation parameters. Usually, underbalanced scenarios are preferred where the wellbore pressure is lesser than the pore pressure during perforation for easy flow of fluids. The reservoir was defined as having a permeability of 1.613 mD and porosity of 0.1454, while the reservoir pore pressure was 8700 Psi. The input parameters of the reservoir and wellbore are shown in Table 2.

A cylindrical wellbore geometry was constructed with a 0.125 m radius, and perforations were distributed in the spiral plane. Ten sets of standard perforations were constructed, having phase angles of 36 degrees each, and fluid flow was simulated using the actual field conditions. Simulating the model and solving it with Darcy's equations gives the directional fluid velocities and the pressure isosurface. Critical draw down obtained previously was used to simulate the fluid flow in a different set of perforations. Major geometrical parameters that determine the flow efficiency in perforated completion are varied. Next, the orientation of the perforation including the phase angle and perforation diameter was varied to study the effect of fluid flow in it. The entire modeling procedure is mentioned in Fig. 5.

Fig. 9 a. Well log representation of critical draw down pressure (CDDP) at different depletion percentage for the studied well taking input as (from extreme left) Gamma (GR) ray log, Sonic (DT) log, Neutron (NPHI) porosity and Density (RHOZ) log, UCS, and stress profile (SHMAX_PHS, SHMIN_PHS, PPRS_EATON_S_2, SVERTICAL_EXT) followed by CDDP (extreme right). **b.** In-depth analysis of similar well 3 at depth 3625–3645 m is represented, respectively



Results

Formation evaluation

SEM images for the core disk were studied and further analyzed to obtain an average grain size. The histogram plots illustrate an average size distribution of 100 μm in the studied core plugs. Figure 6 shows the photomicrograph (SEM images) along with the average grain size distribution represented via histogram.

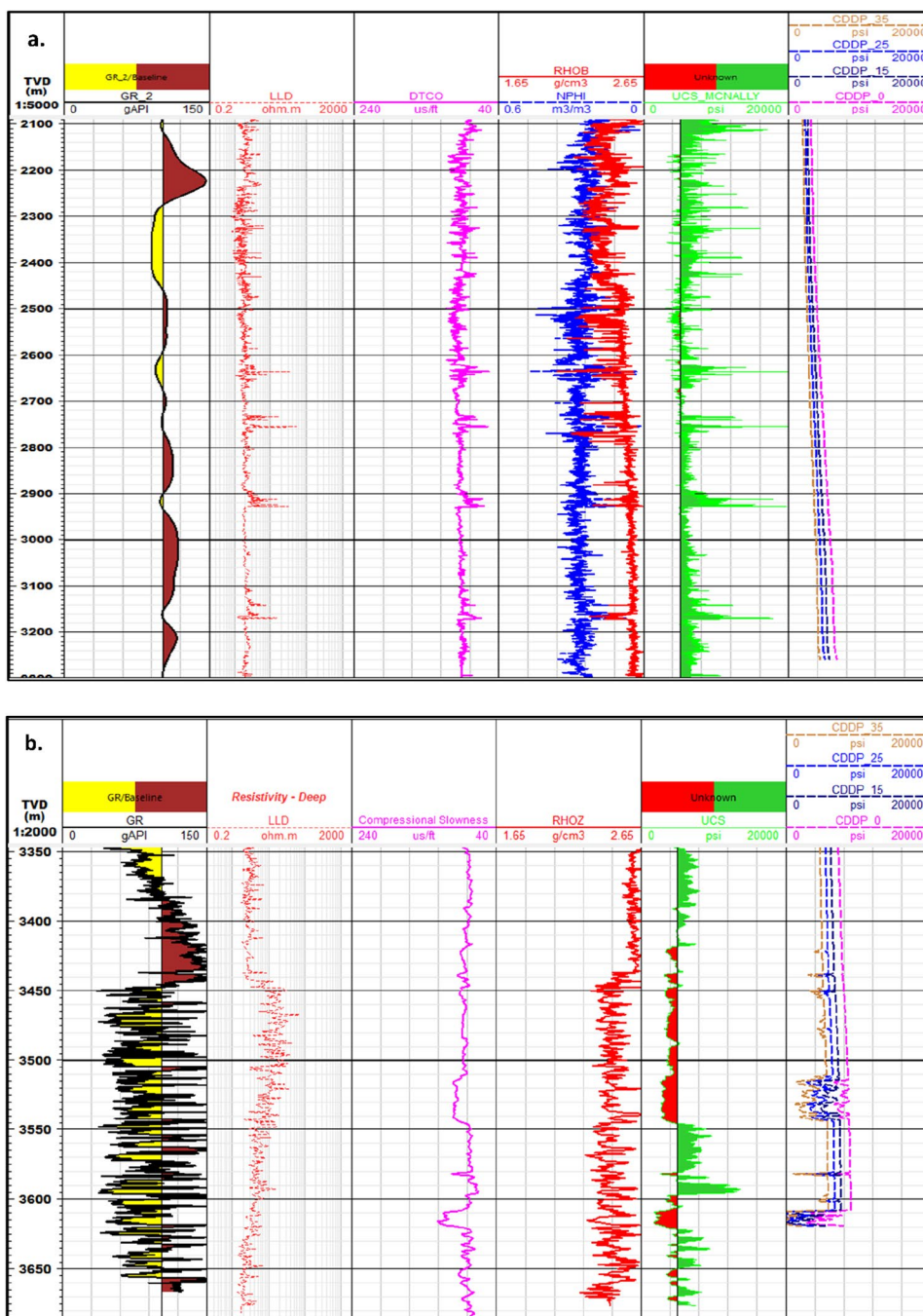
Porosity as inferred from Helium porosimeter shows an average porosity and grain density as given in Table 3. On

an average, lesser porosity of the core plugs makes it more consolidated.

Rock strength properties

UCS is a crucial parameter representing formation strength and an indicator for resisting easy disintegration of sand, therefore slowing the process to the damage to the well by means of less or delayed sand production. Well 3 has a narrow distribution of unconfined compressive strength lying from 500 to 5000 Psi while well 1 has lesser number of samples lying between 5000 and 10,000 Psi. Generally, formations within the well 1 possess enough strength

Fig. 10 Well log representation of critical draw down pressure (CDDP) at different depletion percentage for the studied well taking input as (from extreme left) gamma ray log (GR), resistivity log (LLD), sonic log (DTCO), neutron porosity (NPHI), density log (RHOB), and UCS for well 1 and 2 represented by **a** and **b**, respectively



while well 3 have some areas with relatively lesser strength which could be prone to sanding. Histogram representing the distribution of UCS is shown in Fig. 7.

Cohesion

Cohesion parameter for the studied wells is shown using histogram (Fig. 8), and it was observed that the frequency of samples was relatively higher with lesser magnitudes in

well 3, relative to other wells having a higher magnitude and lesser frequency of samples.

Sanding technique

Sanding analysis quantifies sand production dependence on reservoir pore pressure depletion and drawdown pressure. Critical drawdown profile was created at initial reservoir pore pressure at different percentage of depletion for the studied wells. Density and neutron porosity log helps

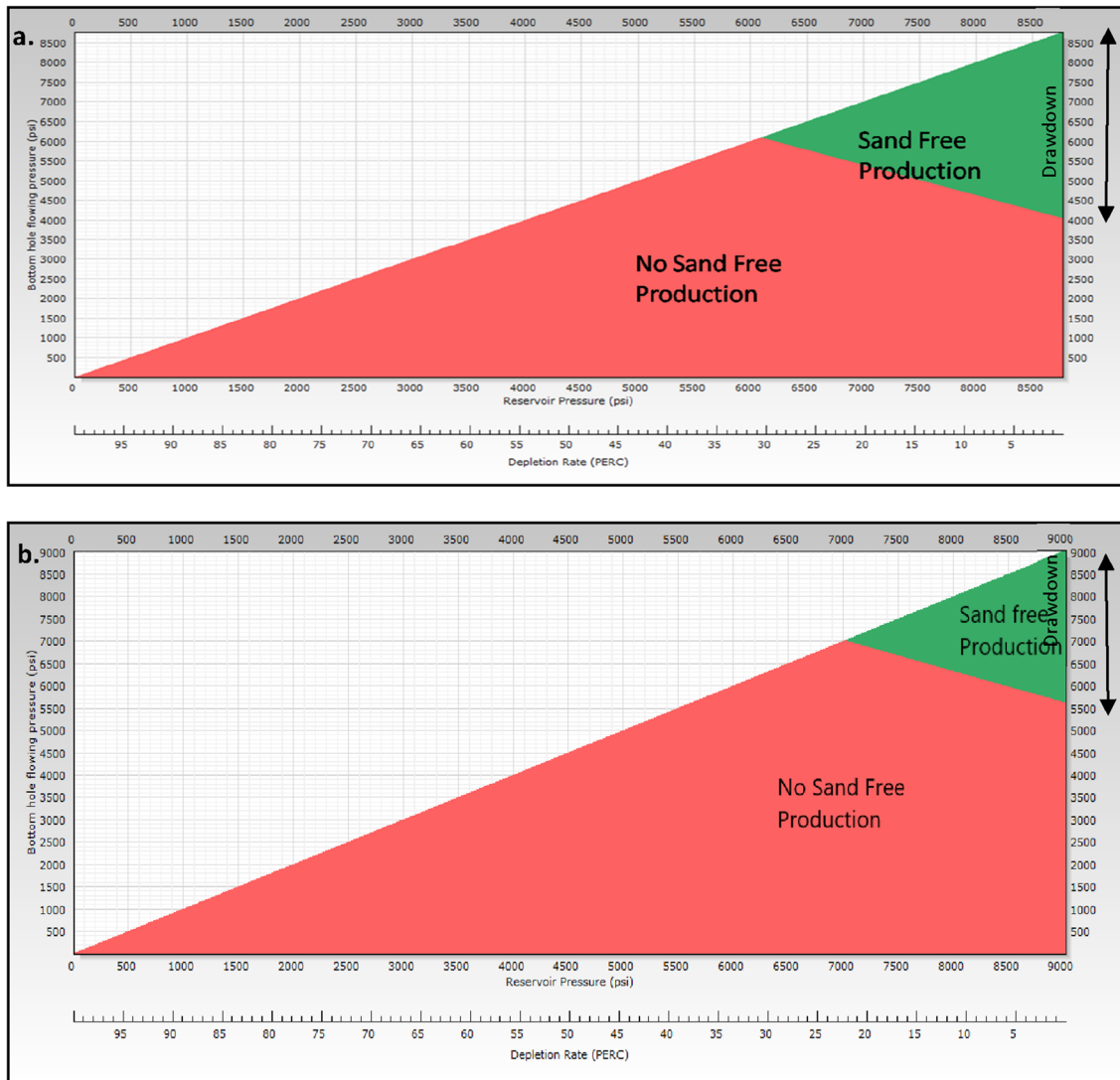


Fig. 11 Cross-plot between the bottom hole pressure and reservoir pore pressure for well 2 and 3 as represented by **a** and **b**, respectively. As reservoir depletion progresses, the reservoir pore pressure decreases, causing the CDDP to decrease as well

Table 4 Critical bottom hole flowing pressure and CDDP for reservoir pore pressure in the studied well 2 and 3 at 0% depletion, respectively

Well no	Critical bottom hole flowing pressure (Psi)	Critical draw down pressure (CDDP) (Psi)
2	4050	4650
3	5600	3400

to differentiate sands from shale while UCS gave an estimation of formation strength. Overlapping of bulk density and neutron porosity in region ‘D’ infers sand formation. Relatively higher UCS indicates that reservoir formation is competent enough to maintain a sand-free production for all depletion considered throughout the life cycle of a well.

There are some limited intervals in well 3 the hydrocarbon producing region that was further well observed in detail as shown in Fig. 9. It was not expected to produce significant volume of sand during production for well 1 as observed in Figs. 9 and 10

Sand risk analysis

Cross-plot has been analyzed for well 2 and 3 for hydrocarbon bearing region showing sanding, as shown in Fig. 11. Well 2 and 3 at certain depth faces sanding. At that depth, a sensitivity analysis is conducted to check for the suitable range of critical bottom hole pressure and critical draw down pressure, for a given reservoir pore pressure at 0% depletion. In well 2, at 0% depletion, the reservoir pore pressure is 8700 psi, whereas the critical bottom hole pressure at the

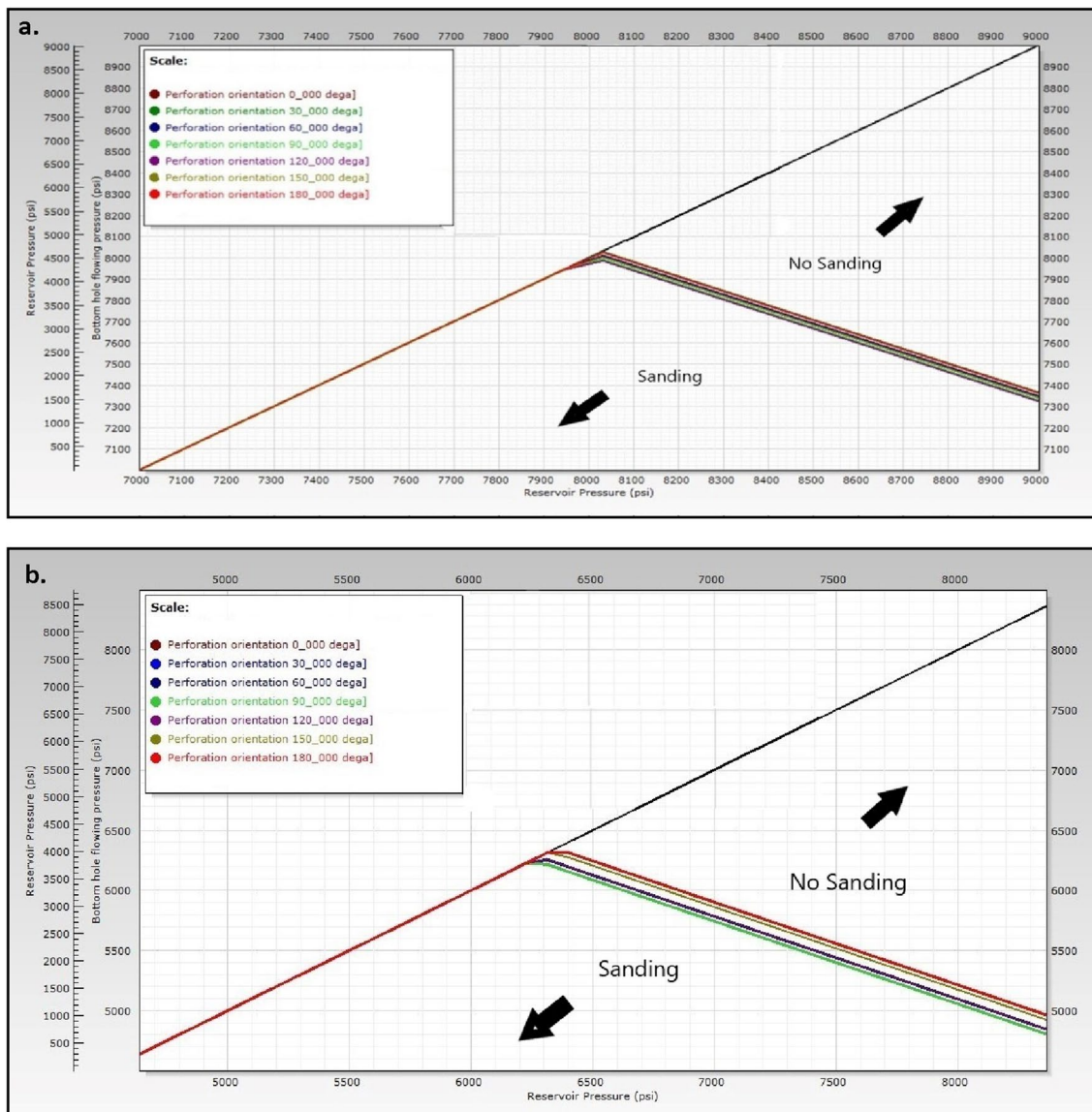


Fig. 12 Sensitivity analysis for well 2 and 3 at different perforation orientations (0°, 30°, 60°, 90°, 120°, 150°, 180°) to check the safe windows for bottom hole pressure as represented by **a** and **b**, respectively

start of production is 4050 Psi. Critical drawdown pressure is the difference between critical bottom hole pressure and reservoir pore pressure, which is 4650 Psi. As reservoir depletion progresses, the reservoir pore pressure decreases, causing the CDDP to decrease as well. When the reservoir pore pressure reaches 6100 Psi, any drawdown will pose a sanding risk.

Similarly, for well 3, the drawdown window diminishes as depletion progresses, and when the reservoir pore pressure strikes 7000 Psi sanding commences. The observations are well tabulated in Table 4 for both wells.

Sand production can be cut down with the help of different perforation parameters like size and orientations

(Cosad 1992). Tendency for sanding was scrutinized using perforations at different set of orientations ranging from 0 to 180 degrees by conducting a sensitivity analysis in the studied wells. For well showing some indications of sanding were further studied at different sets of orientations. It was observed that the 180 or horizontal orientations were less prone to sanding compared to vertical perforations. Not much variation was obtained for well 2, but for well 3 bottom hole window was observed to increase at different orientations as shown in Fig. 12.

Also, the size of the perforations was varied to check for the feasibility of sanding. Standard sizes of 0.5 inch and 1 inch were simulated. The findings reveal that perforation size

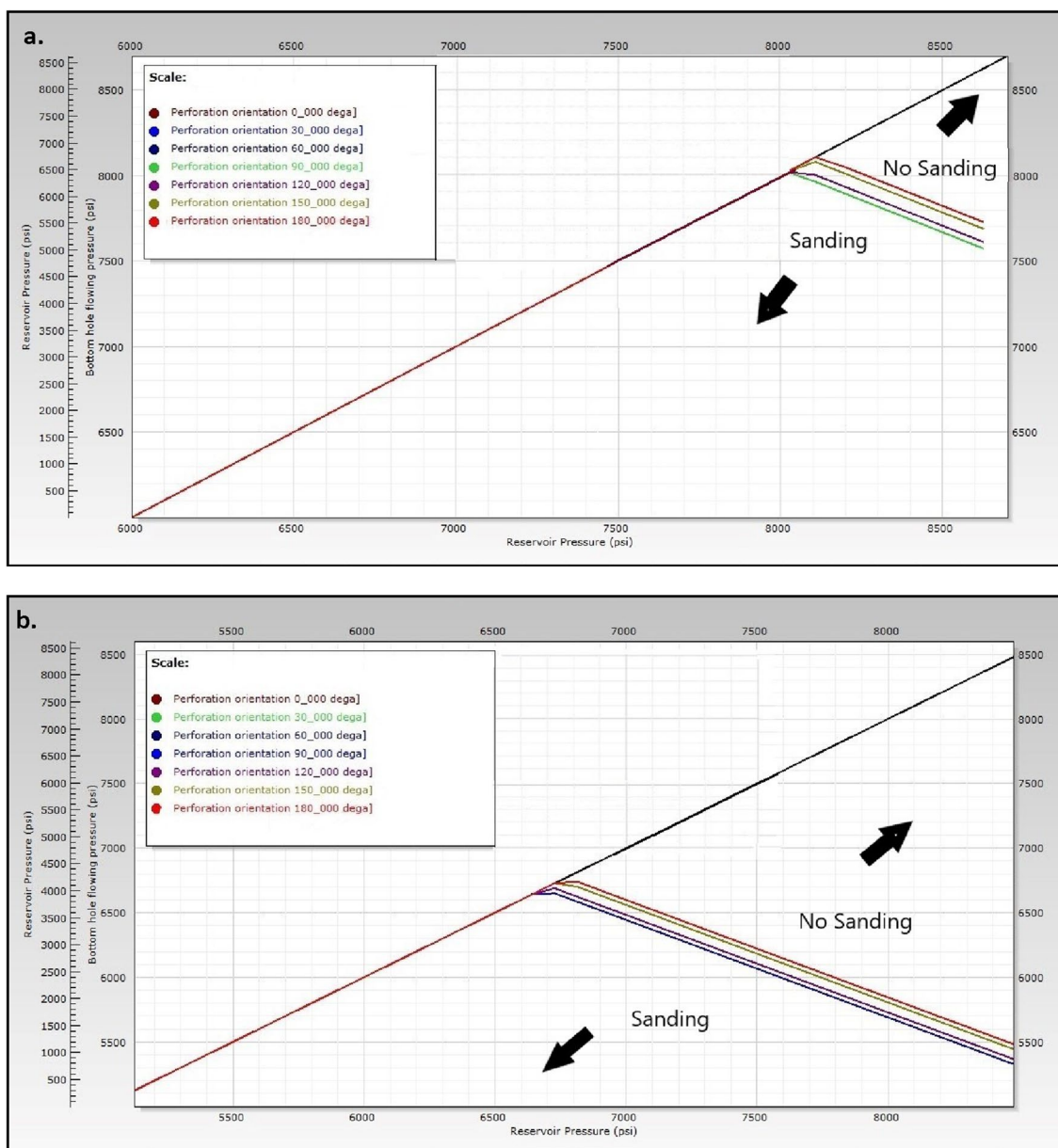


Fig. 13 Cross-plot between bottom hole pressure and reservoir pore pressure for different perforation sizes at similar depth and parameters, **a.** 1 inch perforation diameter, **b.** 0.5 inch perforation diameter

dictates drawdown pressure behavior and varies inversely with the safe windows. A smaller perforation diameter of 0.5 inch lays a broader range of bottom hole pressure than a larger perforation diameter of 1 inch. At a size of 1 inch, the critical drawdown pressure lies within a range of 900–1100 Psi; for 0.5 inch, the CDDP rises to 3100–3300 Psi, as observed in Fig. 13. A wider range of bottom hole windows is available for smaller perforation sizes, and the reservoir will take time to deplete. On the other hand, drawdown is attained soon with increasing depletion for perforations of larger diameter.

Fluid flow simulation using varying drawdown percentage and oriented perforations

The Nandigama formation being the hydrocarbon producing region was simulated with similar petrophysical and lithological attributes for fluid flow from the reservoir to the well. The fluid flow was modeled in porous media having lesser permeability with varying set of oriented perforations. Darcy's law was preferable and was used in the simulation since the major driving force for the flow was pressure gradient and the momentum transfer by the shear stress within

Fig. 14 **a** Well of radius 0.125 m with different set of perforation is defined and its radial distance from the reservoir (2 m) is shown below which is meshed into discrete finite elements. **b.** Represents the flow of fluid from the reservoir (periphery) to well (in the center) via perforations. The reservoir is spread at a distance of 2 m from the well. The flow direction is shown with the help of arrows and the speed of fluid flow is shown with the help of color bar. The speed of fluid flow is maximum at the periphery and decreases as it reaches the well for Nandigama formations

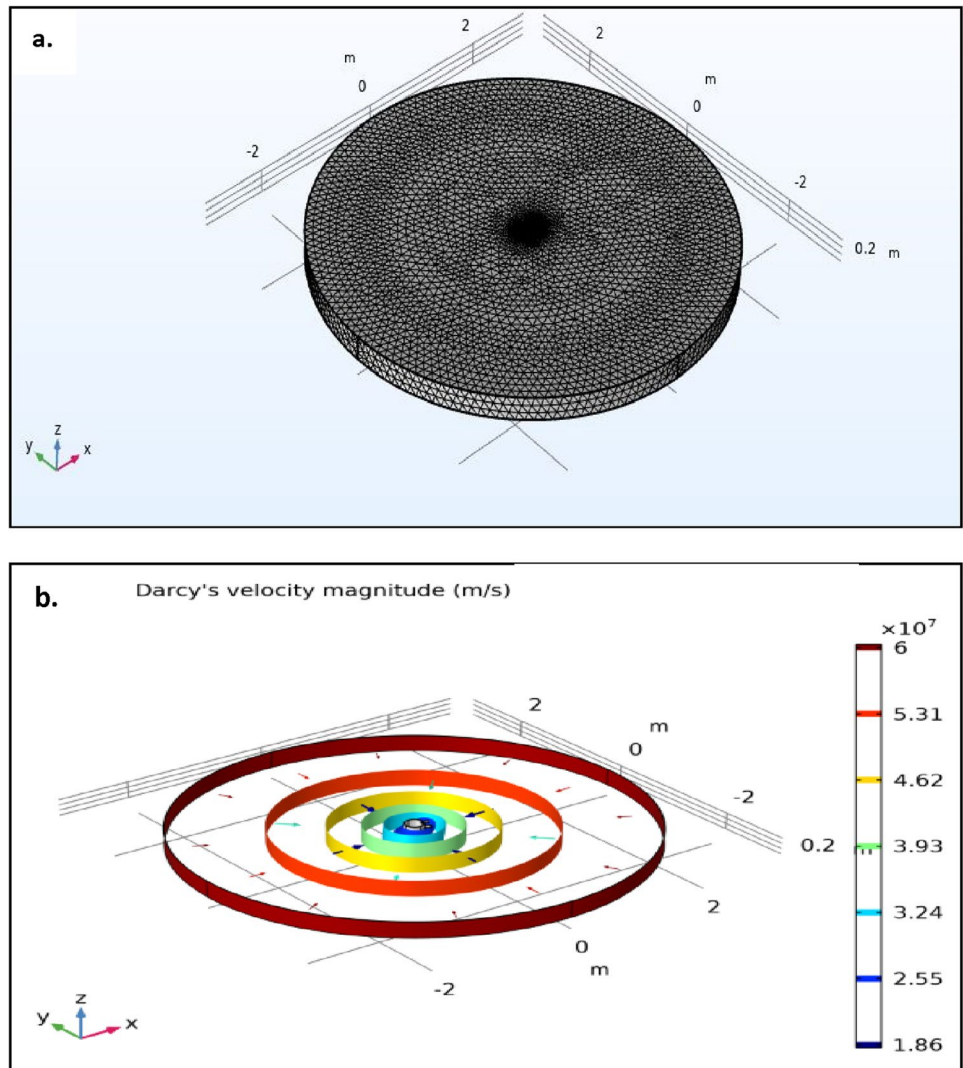


Fig. 15 Cylindrical wellbore having 10 set of perforations oriented at different direction from 0° to 360° is illustrated with the fluid flow rates (from reservoir to well) mentioned at the perforation and tabulated in Table 5

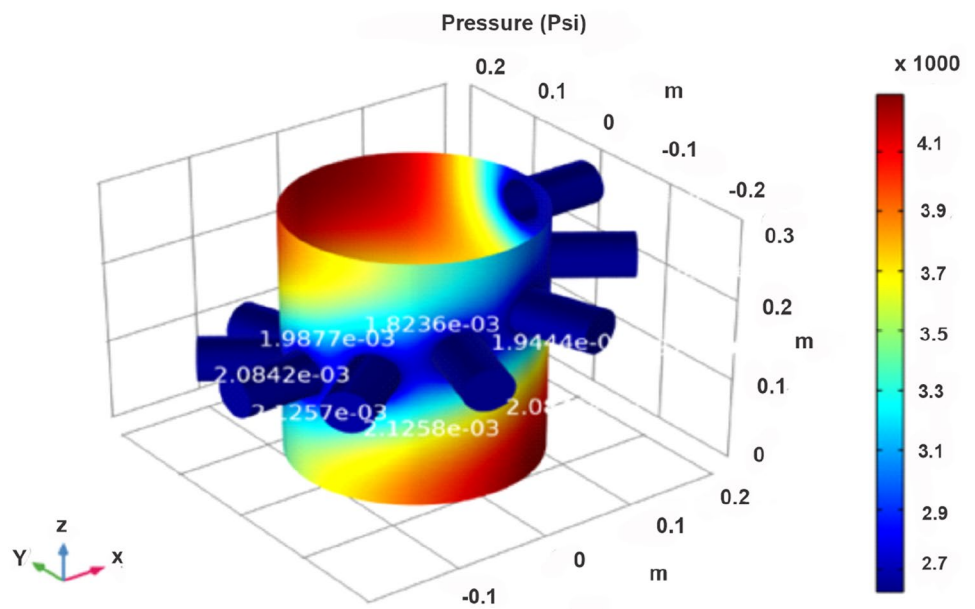


Table 5 Represents the flow rates at different orientation of perforations for the studied formation

Reservoir	Flow rates (m ³ /sec)	Orientation (°)
Nandigama formation	0.002397	0
	0.002248	36
	0.002451	72
	0.002622	108
	0.002571	144
	0.002622	180
	0.002622	216
	0.002571	252
	0.002451	288
	0.002248	324
0.002397	360	
Average fluid flow rate	0.002458	

the fluid was generally negligible. The constructed wellbore model involves geometrical radius of 0.125 m with creation of high resolution grid to capture detailed fluid flow

redistribution. The meshed surface along with the Darcy velocity and isopressure surface is represented in Fig. 14a, b. The reservoir was tested for different number of perforations taken to calculate the pump rate for each case.

Varying set of perforation at different orientation was also studied to understand the influence of fluid production on it (Table 4). Also, the pressure developed at perforation was analyzed via the color scale and rate of fluid flow in the wellbore is shown in Fig. 15. Flow model was simulated using the actual field conditions in Nandigama formation (Kukshal et al. 2022). The reservoir pore pressure for Nandigama formation was calculated as 8702.26 Psi. Flow rates were computed using finite element method and were measured as 0.024548 m³/sec which lies in alignment to the gas flow rate as observed in the studied formation shown in Table 5.

The flow rate was observed to vary with increased size and orientation of perforations. High perforation density with reduced phasing or a greater number of perforations can increase flow efficiency. For increased production of hydrocarbon, it was estimated that the perforation at 180°

Table 6 Represents flow rates at different set of depletion with corresponding draw down pressure as marked in Fig. 16

Depletion	Reservoir pore pressure (Psi)	Bottom hole pressure (Psi)	Draw down pressure (Psi)	Flow rates(m ³ /sec)
10%	8000	4700	3300	0.01639
15%	7500	5200	2300	0.01434
25%	6500	5700	800	0.01229

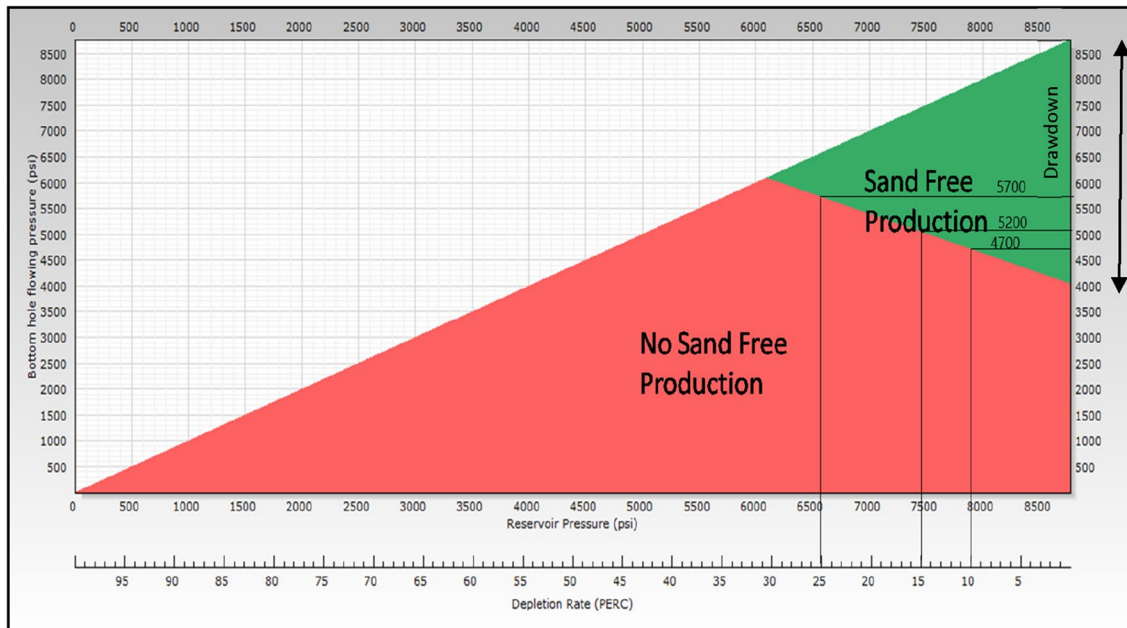


Fig. 16 Illustrates the reservoir pore pressure at different rates of depletion and its corresponding draw down pressure. Depletion is marked as 0, 10, 15 and 25% and flow rates are simulated for the same

has higher flow rates while vertical has relatively lower rates.

At different percentage of depletion, drawdown was set for the fluid flow as mentioned in Table 6. Critical draw down pressure that acts as onset for sanding to occur was inferred and flow rates were calculated for the same as shown in Fig. 16.

Fluid flow rates prior to which sanding occur was calculated as 0.01229 (m³/sec). For enhanced production of hydrocarbon and increased likelihood for hydrocarbon to intersect productive zones, it is suitable to use increased perforation with decreased phasing of lesser diameter as similarly observed by Cosad (1992). It was observed that nearly horizontal orientation with reduced diameter enhances the fluid flow rates.

Conclusions

Sand production is an intricate interplay between fluid flow, reservoir formation strength, and in situ stresses. Unconsolidated sandstone reservoirs with greater porosity are susceptible to sand production, which starts during the first flow or subsequent flows when pore pressure has fallen, or the water breakthrough happens. However, sand production can be completely avoided by selective perforation in stronger regions and oriented perforations (Cosad 1992; Bell 1984). Perforation can be oriented in accordance with the in situ stresses and formation strength condition, in the direction which enhances flow rates without compromising on sand production. Sand production from reservoir formations starts when the reservoir fluid flow transcends a certain threshold influenced by factors, for instance, stress state, consistency of the formation grain, and the completion strategy used around the well.

A detailed study of sanding is undertaken in the KG Basin region to get an insight into the area possessing an inclination to sand production.

- Sand grain diameter was estimated through the histogram plots obtained from the photomicrographs, which shows most of the grain size as 100 μm.
- Critical draw down pressure (CDDP), which is a function of both critical bottom hole pressure and reservoir pore pressure, for well 1 and well 2 is estimated as 4650 Psi and 3400 Psi, respectively, at 0% depletion.
- A finite element model was simulated with similar petrophysical characteristics to that of studied formation for investigating the fluid flow rates which were numerically calculated as 0.024548 m³/sec.

- Depth sections prone to sanding were further investigated to estimate the range of bottom hole pressure for corresponding reservoir pore pressure at different depletion percentage and fluid flow rates were calculated. At depletion percentage of 25%, critical fluid flow rates were calculated as 0.01229 (m³/sec).
- Further, fluid flow rates were calculated using different orientations and sizes and it was observed that the production rates were enhanced at horizontal perforation. It was also observed that fluid flow rates were relatively increased in horizontal perforation of lesser diameter.

This study will be helpful in computing realistic production rates for feasible completion options. An implementation will save time and money and can be used to calculate sand-free production in basins with similar complexity and heterogeneity.

Acknowledgements The authors are thankful to Department of Earth Sciences, IIT Roorkee, and the management of Oil and Natural Gas Corporation Ltd. at KDMIPE, Dehradun, for providing resources and support to publish this paper. The views expressed in this paper are of the authors only and may not necessarily be of the organizations they belong to.

Author contributions AK (First Author) contributed to methodology, investigation, formal analysis, validation, and writing—original draft. RS (Corresponding Author) contributed to conceptualization, supervision, resources, visualization, and writing—review and editing. HJK (co-author) contributed to data curation, investigation, and writing—review and editing. GMY (co-author) contributed to data curation, investigation, and writing—review and editing. VDJ (co-author) contributed to data curation, investigation, and writing—review and editing. Harilal (Co-Author) contributed to resources, and writing—review and editing.

Funding No funding was received for conducting this study.

Declarations

Conflict of interest The authors have no competing interests to declare that are relevant to the content of this article.

Open Access This article is licensed under a Creative Commons Attribution 4.0 International License, which permits use, sharing, adaptation, distribution and reproduction in any medium or format, as long as you give appropriate credit to the original author(s) and the source, provide a link to the Creative Commons licence, and indicate if changes were made. The images or other third party material in this article are included in the article's Creative Commons licence, unless indicated otherwise in a credit line to the material. If material is not included in the article's Creative Commons licence and your intended use is not permitted by statutory regulation or exceeds the permitted use, you will need to obtain permission directly from the copyright holder. To view a copy of this licence, visit <http://creativecommons.org/licenses/by/4.0/>.

References

- Abdelghany WK, Hamed MS, Radwan AE et al (2023) Implications of machine learning on geomechanical characterization and sand management: a case study from Hilal field, Gulf of Suez. *Egypt J Petrol Explor Prod Technol* 13:297–312. <https://doi.org/10.1007/s13202-022-01551-9>
- Abduljabbar A, Mohyaldinn ME, Younis, et al (2022) Erosion of sand screens by solid particles: a review of experimental investigations. *J Petrol Explor Prod Technol* 12:2329–2345. <https://doi.org/10.1007/s13202-022-01467-4>
- Ahad NA, Jami M, Tyson S (2020) A review of experimental studies on sand screen selection for unconsolidated sandstone reservoirs. *J Petrol Explor Prod Technol* 10:1675–1688. <https://doi.org/10.1007/s13202-019-00826-y>
- Aroyehun ME, Oko F, Onyeansi O, Oguntade T, Kabara A, Dimkpa B (2018) Comparative study of sand control methods in selected Niger-delta sandstone reservoirs SPE Nigeria Annual International Conference and Exhibition. *Soc Petrol Eng.* <https://doi.org/10.2118/193526-MS>
- Krishna Godavari Basin, National data repository, director general of Hydrocarbons (2022)
- Bastia R, Nayak P, and Singh P (2006) Shelf delta to deepwater basin: a depositional model for Krishna Godavari basin. In: AAPG International Conference, Perth, West Australia, Article #40231, November 5–8
- Bell WT (1984) Perforating underbalanced- evolving techniques, *journal of petroleum technology*. No 10:1653–1662. <https://doi.org/10.2118/13413-PA>
- Bowes C, Procter R (1997) *Drillers stuck pipe handbook, guidelines & drillers handbook credits Schlumberger, Ballater, Scotland*
- Cosad C (1992) Choosing a perforation strategy. *Oilfield Reviews* 4(4):54–69
- Crawford HR (1989) Underbalanced perforating design, paper SPE 19749, presented at the SPE annual technical conference and exhibition. San Antonio, Texas, USA. <https://doi.org/10.2118/19749-MS>
- Dehghani F (2016) Sand production management for oil and gas reservoirs 2016-Sustainable Industrial Processing Summit, Floren Star Outreach, pp 363–370
- Deng F, Deng J, Yan W et al (2013) The influence of fine particles composition on optimal design of sand control in offshore oilfield. *J Petrol Explor Prod Technol* 3:111–118. <https://doi.org/10.1007/s13202-012-0045-7>
- Deng F, Shen X, Liang Q et al (2018) The jamming mechanism of sand control screen for the montmorillonite inflation with the water. *J Petrol Explor Prod Technol* 8:189–194. <https://doi.org/10.1007/s13202-017-0329-z>
- Haimson BC, Chang C (2000) A new true triaxial cell for testing mechanical properties of rock, and its use to determine rock strength and deformability of Westerly granite. *Int J Rock Mech Min Sci* 37:285–296
- Heidbach O, Rajabi M, Cui X, Fuchs K, Müller B, Reinecker J, Reiter K, Tingay M, Wenzel F, Xie F, Ziegler MO, Zoback MD (2018) The world stress map database release 2016: crustal stress pattern across scales. *Tectonophysics* 744:484–498. <https://doi.org/10.1016/j.tecto.2018.07.007>
- Ismail NI, Naz MY, Shukrullah S et al (2020) Mechanical earth modeling and sand onset production prediction for Well X in Malay Basin. *J Petrol Explor Prod Technol* 10:2753–2758. <https://doi.org/10.1007/s13202-020-00932-2>
- Issa MA, Hadi FA, Nygaard R (2022) Coupled reservoir geomechanics with sand production to minimize the sanding risks in unconsolidated reservoirs. *Pet Sci Technol* 40(9):1065–1083. <https://doi.org/10.1080/10916466.2021.2014522>
- Jin Y, Chen J, Chen M et al (2012) Experimental study on the performance of sand control screens for gas wells. *J Petrol Explor Prod Technol* 2:37–47. <https://doi.org/10.1007/s13202-012-0019-9>
- Kidambi T, Kumar GS (2016) Mechanical Earth Modeling for a vertical well drilled in a naturally fractured tight carbonate gas reservoir in the Persian Gulf. *J Petrol Sci Eng (elsevier Publ)*. <https://doi.org/10.1016/j.petrol.2016.01.003>
- Kukshal A, Sharma R, Jamwal VD, Yeshwanth GM (2022) Determination of in-situ stress using elastic parameters and pore pressure in unconventional shale formations of the Indian eastern onshore basin. In: ARMA US Rock Mechanics/Geomechanics Symposium (pp ARMA-2022). ARMA. <https://doi.org/10.56952/ARMA-2022-0326>
- Lacy LL (1997) Dynamic rock mechanical testing for optimized fracture designs. *SPE Paper*. <https://doi.org/10.2118/38716-MS>
- Li J, Wei J, Zhou X et al (2022) Influence of proppant physical properties on sand accumulation in hydraulic fractures. *J Petrol Explor Prod Technol* 12:1625–1632. <https://doi.org/10.1007/s13202-021-01423-8>
- Madadzadeh A, Sadeghein A, Riahi S (2022a) The use of nanotechnology to prevent and mitigate fine migration: a comprehensive review. *Rev Chem Eng.* <https://doi.org/10.1515/REVCE-2019-0055/HTML>
- Madadzadeh A, Sadeghein A, Riahi S (2022b) A Comparison of different nanoparticles' effect on fine migration by low salinity water injection for oil recovery: introducing an optimum condition. *J Energy Resour Technol Trans ASME.* <https://doi.org/10.1115/1.4052415/1119507>
- Madadzadeh A, Sadeghein A, Riahi S (2022c) Effects of nanosilica on fine migration and location distribution of blockage at different pH and temperatures: Modelling and experimental studies. *Can J Chem Eng.* <https://doi.org/10.1002/cjce.24353>
- Mahmud HB, Leong VH, Lestario Y (2020) Sand Production: a smart control framework for risk mitigation. *Petroleum* 6(2020):1–13. <https://doi.org/10.1016/j.petlm.2019.04.002>
- Mahmud HB and Abdullah A (2017) Investigate a gas well performance using nodal analysis In: International Conference on Materials Technology and Energy, Curtin University Malaysia, pp 20–21
- Matanovic D, Cikes M, and Moslavac B (2012) *Sand Control in Well Construction and Operation*, Springer Science and Business Media. ISBN 9783642 256134
- McLellan PJ, Hawkes CD, Read RS (2000) Sand Production Prediction for Horizontal Gas Storage Wells SPE/PS-CIM 65510 presented at the 2000 SPE/Petroleum Society of CIM International Conference on Horizontal Well Technology, Calgary, Alberta, Canada, 6–8 November, SPE 65510/PS2000–149
- Moore WR (1994) (1994) Sand Production Prediction. *J Petrol Technol* 46(11):955–955. <https://doi.org/10.2118/29331-pa>
- Morita N and Boyd PA (1991) Typical Sand Production Problems: Case Studies and Strategies for Sand Control, paper SPE 22739 presented at the 1991 SPE Annual Technical Conference and Exhibition, Dallas, TX, 6–9 October
- Papamichos E, Vardoulakis I, Tronvoll J, Skjaerstein A (2001) Volumetric sand production model and experiment. *Int J Numer Anal Methods GeoMech* 25:789–808
- Pearson JRA and Zazovsky AF (1997) A model for the transport of sand grains from a perforation during underbalance surge, SPE 38634. In: Proceedings of SPE Annual Technical Conference and Exhibition, San Antonio, TX, U.S.A, October, 1997
- Plumb RA, Herron SL, and Olsen MP (1992) Influence of Composition and Texture on Compressive Strength Variations in the Travis

- Peak Formation. In: 67th Annual Technical Conference and Exhibition, SPE, Washington, D.C. SPE 24758
- Plumb RA (1994) Influence of composition and texture on failure properties of clastic rocks, SPE-28022-MS. <https://doi.org/10.2118/28022-MS>
- Rahman K, Khaksar A, Kayes TJ (2010) An integrated geomechanical and passive sand-control approach to minimizing sanding risk from openhole and cased-and-perforated wells. *Soc Petrol Eng* 25(2):155–167. <https://doi.org/10.2118/116633-PA>
- Rahmati H, Jafarpour M, Azadbakht S, Nouri A, Vaziri H, Chan D, Xiao Y (2013) Review of sand production prediction models. *J Petrol Eng*. <https://doi.org/10.1155/2013/864981>
- Rao GN, Mani KS (1993) A study on generation of abnormal pressures in Krishna-Godavari basin. *Indian J Petrol Geol* 2:20–30
- Salahi A, Dehghan AN, Sheikhzakariaee SJ, Davarpanah A (2021) Sand production control mechanisms during oil well production and construction. *Petrol Res* 6:361–367
- Sanfilippo F, Ripa G, Brignoli M, and Santarelli FJ (1995) Economical management of sand production by a methodology validated on an extensive database of field data, paper SPE 30472 presented at the 1995 SPE Annual Technical Conference and Exhibition, Dallas, TX, 22–25 October
- Subbiah SK (1997) Wellbore instability studies by physical modeling. Universiti Teknologi Malaysia. M. Eng. Thesis
- Sulaimon AA, Teng LL (2020) Modified approach for identifying weak zones for effective sand management. *J Petrol Explor Prod Technol* 10:537–555. <https://doi.org/10.1007/s13202-019-00784-5>
- Tabar MA, Bagherzadeh H, Shahrabadi A et al (2021) A comprehensive research in chemical consolidator/stabilizer agents on sand production control. *J Petrol Explor Prod Technol* 11:4305–4324. <https://doi.org/10.1007/s13202-021-01303-1>
- Tovar J (2018) Characterization of lower sand control completion failure in oil wells In: 80th EAGE Conference and Exhibition 2018, European Association of Geoscientists and Engineers, pp 1–5
- Tremblay B, Sedgwick G, and Forshner K (1996) Imaging of sand production in a horizontal sand pack by X-ray computed tomography, SPE formation Evaluation, 94–98, SPE-30248-PA. <https://doi.org/10.2118/30248-PA>
- Tronvoll J, Skjærstenin A, Papamichos E (1997) Sand production: mechanical failure or hydrodynamic erosion. *Int J Rock Mech Min Sci* 34(3–4):853–862
- Vardoulakis I, Stavropoulou M, Papanastasiou P (1996) Hydro-mechanical aspects of the sand production problem. *Transp Porous Media* 22(2):225–244
- Vaziri HH, Lemoine EM, Xiao Y (2002) Quantification of sand production induced improvement in productivity index. *Can Geotech J* 39:1088–1102
- Vaziri HH, Thallak S, and Phillips R (1998b) Investigation of sand production mechanisms resulting in enhanced cold production. In: Proceedings of International Society of Soil Mechanics and Foundation Engineering Centrifuge
- Vincent ON, Abiola SO, Felix OO, and Ajenka JA (2012) Sanding in Oil Well Reservoir Completions in SPE Nigeria Annual International Conference and Exhibition. SPE, 163010-MS
- Wang J, Walters D, Settari A, and Wan RG (2006) An integrated modular approach to modeling sand production and cavity growth with emphasis on the multiphase flow and 3D effects. In: Proceedings of the 41st U.S. Symposium on Rock Mechanics Symposium, Golden, Colo, USA
- Weigarten JS, Perkins TK (1995) Prediction of sand production in gas wells: methods and gulf of mexico case studies, *JPT*, 596–600, SPE 24797. <https://doi.org/10.2118/24797-PA>
- Willson S, Moschovidis ZA, Cameron J., Palmer I. (2002) New model for predicting the rate of sand production. In: Proceedings of the SPE/ISRM Rock Mechanics Conference, Irving, Tex, USA, October 2002, <https://doi.org/10.2523/78168-MS>
- Yan C, Li Y, Cheng Y, Wang W, Song B, Deng F, Feng Y (2018) Sand production evaluation during gas production from natural gas hydrates. *J Nat Gas Sci Eng* 57:77–88
- Zhang J (2011) Pore pressure prediction from well logs Methods, modification and new approaches. *Earth-Sci Rev* 108(1–2):50–63
- Zhang H, Pu C, Wang Y, Sun C (2020) Experimental and Numerical Investigation on Influence of Pore-Pressure Distribution on Multi-Fractures Propagation in Tight Sandstone, *Engineering Fracture Mechanics*, Article 106993
- Zhu M, Yu L, Zhang X, Davarpanah A (2020) Application of implicit pressure-explicit saturation method to predict filtrated mud saturation impact on the hydrocarbon reservoirs formation damage. *Mathematics* 8(7):1057
- Zolotukhin AB, Gayubov AT (2022) Analysis of nonlinear effects in fluid flows through porous media. *J Petrol Explor Prod Technol* 12:2237–2255. <https://doi.org/10.1007/s13202-021-01444-3>

Publisher's Note Springer Nature remains neutral with regard to jurisdictional claims in published maps and institutional affiliations.